Transport of localized and extended excitations in chains embedded with randomly distributed linear and nonlinear *n*-mers

Dany López-González and Mario I. Molina
Departamento de Física, MSI-Nucleus on Advanced Optics, and Center for Optics and Photonics (CEFOP), Facultad de Ciencias, Universidad de Chile, Santiago, Chile

(Received 28 June 2015; revised manuscript received 20 November 2015; published 7 March 2016)

We examine the transport of extended and localized excitations in one-dimensional linear chains populated by linear and nonlinear symmetric identical n-mers (with $n = 3, 4, 5$, and 6), randomly distributed. First, we examine the transmission of plane waves across a single linear n-mer, paying attention to its resonances, and looking for parameters that allow resonances to merge. Within this parameter regime we examine the transmission of plane waves through a disordered and nonlinear segment composed by n-mers randomly placed inside a linear chain. It is observed that nonlinearity tends to inhibit the transmission, which decays as a power law at long segment lengths. This behavior still holds when the n-mer parameters do not obey the resonance condition. On the other hand, the mean square displacement exponent of an initially localized excitation does not depend on nonlinearity at long propagation distances z, and shows a superdiffusive behavior $\sim z^{1.8}$ for all n-mers, when parameters obey the resonance merging condition; otherwise the exponent reverts back to the random dimer model value $\sim z^{1.5}$.

DOI: 10.1103/PhysRevE.93.032205

I. INTRODUCTION

One of the staples of modern condensed matter physics is the well-known phenomenon of Anderson localization [1,2]. Roughly speaking it asserts that the presence of disorder tends to localize the eigenfunctions of the system, thus impeding the transport of excitations across it. In one and two dimensions any amount of disorder will suffice to render all eigenfunctions localized, causing a complete lack of transport. In three-dimensional systems, there is a mobility edge separating the localized from the extended wave functions. The Anderson result was originally derived for a system of independent electrons in the tight-binding approximation which are subject to diagonal or off-diagonal disorder. A direct observation of Anderson localization in a solid is hard since there are many other competing effects: electron-electron interactions, phonons, electron-phonon interactions, point and extended defects, etc. However, there are other systems that fall outside condensed matter and that can be described by tight-binding-like equations. One example is optical waveguide arrays [3]. Usually, these arrays consist of dielectric channels put in close proximity to each other forming a geometric array in one or two dimensions. Each channel supports a single electromagnetic mode and the overlapping of the evanescent field of these modes gives rise to a transverse dynamics, described by discrete equations, which are formally identical to the tight-binding model equations. In fact, it was in this optical analog that Anderson localization in one and two dimensions was observed for the first time [4,5]. The reason is clear: In the optical analog it is possible to introduce diagonal disorder by simply changing the index of refraction of the guides, and off-diagonal disorder is produced by changing the coupling (distance) between guides. There are no other encumbering effects like those encountered in a condensed matter setting.

Now, Anderson localization is based on the assumption that disorder is "perfect" or uncorrelated. However, at the beginning of the 1990s it was noted that, in systems with correlated disorder, a degree of transport was still possible [6–8]. For the specific case of correlated diagonal disorder, Dunlap *et al.* examined the localization-delocalization transition for a random dimer model (RDM) consisting of a binary alloy where one of the site energies is assigned at random to pairs of lattice sites. In that case, and if the difference between the site energies is smaller than a half bandwidth, then a number of resonant wave vectors exist for which the localization length of the states exceeds the size of the sample, N, becoming effectively extended. The fraction of the states that become extended in this manner is of the order of $\sqrt{N}$, and this leads to a mean square displacement, of an initially localized excitation, that grows as $t^{3/2}$. This effect has been recently demonstrated experimentally in an optical setting in Ref. [9]. Since then, the RDM has been generalized to include the random trimer model [8], the random dimer-trimer model [10],and the random binary n-mer model [11]. For the particular case of the symmetric trimer, there are two possible resonances and Giri *et al.* analyzed the possibility of merging these two resonances, which has as a consequence an increase of the width of the extended states. In the same vein, Huang *et al.* [12] found that for the symmetric random trimer model there is still diffusion even when the central site energy is random.

In this work we consider a further generalization of this model by considering larger "defects" (tetramers, pentamers, hexamers) and more general symmetric site energy distributions, and also by including nonlinear effects. For the strictly homogeneous n-mer case, we observe the same phenomenology as in the random dimer model. The reason for this behavior is discussed at the end of Sec. III D. Thus, we focus on inhomogeneous but symmetric n-mers, which display interesting transport properties.

This paper is organized as follows: In Sec. II we consider the transmission coefficient of plane waves across a single defect (trimer, tetramer, pentamer, or hexamer) embedded in a homogeneous chain and compute the region of parameters (site energy distribution inside the n-mer) inside which it is possible to adjust the position of the system resonances. In Sec. III we

consider a disordered chain that contains a fraction (50%) of identical n-mer defects, randomly distributed, and examine the transmission coefficient as a function of the length of the disordered region in the presence and absence of nonlinear effects. In Sec. IV we study the transport dynamics of an initially localized excitation, by measuring the asymptotic exponent of the mean square displacement. Also we study the effect of nonlinearity on these exponents. We conclude the paper in Sec. V with a discussion of the main results.

II. THE MODEL

Let us consider a general excitation propagating on a lattice whose dynamics is well described by the discrete nonlinear Schrödinger (DNLS) equation

$$i\frac{d\psi_n}{dz} = \epsilon_n\psi_n + V(\psi_{n+1} + \psi_{n-1}) + \chi|\psi_n|^2\psi_n, \qquad (1)$$

where, in the optics domain, ψ_n is the amplitude of the electric field on the nth waveguide, V is the coupling coefficient between nearest-neighbor guides, ϵ_n is proportional to the index of refraction of waveguide n, and χ is the nonlinear (Kerr) parameter which has to be taken into account at high electric field amplitudes. We look for stationary solutions of the form $\psi_n = C_n e^{iEz}$. After inserting this into Eq. (1), we obtain

$$EC_n + \epsilon_n C_n + V(C_{n+1} + C_{n-1}) + \chi|C_n|^2 C_n = 0. \qquad (2)$$

Note that changing the output amplitude is equivalent to rescaling the nonlinearity coefficient, and vice versa. This is seen from Eq. (2) rewritten as

$$C_{n+1} = -[(E/V) + (\epsilon_n/V) + (\chi/V)|C_n|^2]C_n - C_{n-1}. \qquad (3)$$

Under the scaling $C_n \to \alpha\, C_n$, this relation reads

$$C_{n+1} = -[(E/V) + (\epsilon_n/V) + (\alpha^2\chi/V)|C_n|^2]C_n - C_{n-1}, \qquad (4)$$

which shows that changing C_n is equivalent to changing χ: $C_n \to \alpha\, C_n \Longleftrightarrow \chi \to \alpha^2\chi$. On the other hand, if we change $\chi \to \alpha\chi$, the backward map reads

$$\phi_{n+1} = -[(E/V) + (\epsilon_n/V) + (\chi/V)|\phi_n|^2]\phi_n - \phi_{n-1}, \qquad (5)$$

where $\phi = \sqrt{\alpha}C_n$. That is, changing χ is equivalent to changing C_n: $\chi \to \alpha\chi \Longleftrightarrow C_n \to C_n\sqrt{\alpha}$. This implies that the transmission coefficient gets multiplied by α, $T \to \alpha\, T$. It proves convenient to rewrite Eq. (2) as

$$C_{n+1} = -(E + \epsilon_n + \chi|C_n|^2)C_n - C_{n-1}, \qquad (6)$$

where, without loss of generality, we have taken $V = 1$. This form is useful when considering transmission problems.

Let us now consider a chain segment between $n = 0$ and $n = m$ (m-mer), characterized by a site energy distribution $\{\epsilon_n\}$ and a nonlinear coefficient χ, that is joined on both sides to semi-infinite linear homogeneous chains, characterized by $\epsilon_n = 0 = \chi$. We want to compute the transmission coefficient of plane waves across this segment, or m-mer (see Fig. 1). The incident wave has the form $C_n = r_0\exp[-ik(n-m)] + r_1\exp[ik(n-m)]$ for $n \geqslant m$ (the wave comes "from the right"). The transmitted wave is $C_n = t\exp[ik]$ for $n \leqslant 0$. Initial conditions are $C_0 = t$ and $C_{-1} = t\exp(ik)$, plus

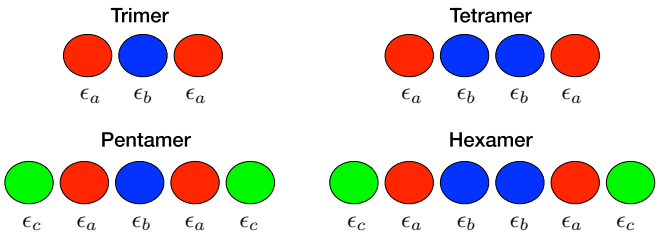

FIG. 1. Site energy distribution of the several n-mers that populate randomly a linear chain.

$E = 2\cos(k)$. Now we resort to Eq. (6) and iterate it until we determine r_0 and r_1. Based on this information, we deduce the form of the transmission and reflection coefficient as

$$T = |t/r_0|^2 = \frac{|e^{2ik} - 1|^2}{|C_{m+1} - e^{-ik}C_{m+2}|^2}, \qquad (7)$$

$$R = |r_1/r_0|^2 = \frac{|C_{m+2} - C_{m+1}e^{-ik}|^2}{|C_{m+1} - e^{-ik}C_{m+2}|^2}, \qquad (8)$$

where C_{m+1} and C_{m+2} are obtained from Eq. (6) by iteration. The condition for a transmission resonance is given by $R = 0$; that is,

$$|C_{m+2} - C_{m+1}e^{-ik}| = 0. \qquad (9)$$

III. THE SINGLE n-MER (IMPURITY) CASE

Let us begin by considering a single linear ($\chi = 0$) n-mer and finding the conditions for transmission resonances to exist. In general there are $n-1$ of them, and we want to find a parameter region where one can "control" said resonances, for instance, to be able to merge two or more of them. As we see later, this has an impact on the transport properties of localized excitations in a disordered medium. The idea is that in a chain populated at random with these n-mers, the curvature around a given resonance determines the number of states whose localization length is greater than the dimensions of the chain. In that case, we have a fraction of states that are effectively delocalized and can give rise to transport (electronic or optical) as shown by Dunlap *et al.* for the case $m = 2$ [7]. For our n-mers we hope that when two or more resonances merge, the curvature around the common resonance will change the number of delocalized states, changing in this manner the asymptotic exponent of the mean square displacement of an initially localized excitation.

A. Symmetric trimer

This case was already examined by Giri *et al.* [8], but we present it here, in a slightly different manner. We consider a segment formed by three sites located at $n = 0$, 1, and 2, with site energies ϵ_a, ϵ_b, and ϵ_a (see Fig. 1). By using Eqs. (7) and (8), we obtain the transmission and reflection coefficient as

$$T = \left|\frac{(-1 + e^{2ik})}{(-1 + e^{2ik}) + e^{3ik}\epsilon_a^2\epsilon_b + e^{ik}B - e^{2ik}C}\right|^2, \qquad (10)$$

$$R = \left|\frac{(1 + \epsilon_a^2)\epsilon_b - A\cos(k) + 2\epsilon_a\cos(2k)}{(-1 + e^{2ik}) + e^{3ik}\epsilon_a^2\epsilon_b + e^{ik}B - e^{2ik}C}\right|^2, \qquad (11)$$

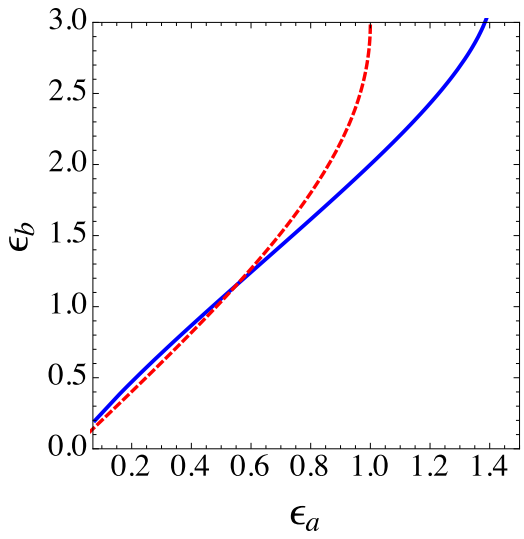

FIG. 2. Parameter curves in $\epsilon_a - \epsilon_b$ plane on which we have merging of two resonances. The trimer curve (dashed line) is obtained from the closed form solution (14), while the one for the tetramer (solid line) is obtained numerical from Eq.(16).

where A, B, and C are listed in the Appendix. The resonance condition (9) leads to the quadratic equation

$$4\cos(k)^2\epsilon_a + \cos(k)\left(-2\epsilon_a^2 - 2\epsilon_a\epsilon_b\right) + \epsilon_b + \epsilon_a^2\epsilon_b - 2\epsilon_a = 0. \tag{12}$$

After solving this equation one finds two resonances

$$\cos(k) = \frac{\epsilon_b + \epsilon_a}{2} \pm \sqrt{p^2 - 4q}, \tag{13}$$

where $p = \epsilon_b - \epsilon_a$ and $q = (\epsilon_b/\epsilon_a) - 2$.

For $p^2 = 4q$ the two resonances merge into a single one [8] when

$$\epsilon_b = \epsilon_a\left[\frac{8 + \epsilon_a^2}{2 + \epsilon_a^2 + 2\sqrt{1 - \epsilon_a^2}}\right], \tag{14}$$

which is analogous to the result obtained previously by Giri *et al.* The case of the homogeneous trimer, $\epsilon_a = \epsilon_b = \epsilon_c$, gives rise to a single resonance only and to transport properties analogous to the ones obtained for the dimer case [7]. Thus, it is not interesting to us and is not discussed here. Figure 2 shows the curve in parameter space where the two resonances merge. The resonance curve ends at $\epsilon_a = 1$, $\epsilon_b = 3$.

B. Tetramer

Now we consider an $n = 4$ segment, with site energies distributed in a symmetric manner as $\epsilon_a\epsilon_b\epsilon_b\epsilon_a$ (see Fig. 1). Proceeding as before, we compute the transmission and reflection coefficients in closed form, obtaining

$$R = \left|\frac{Z - A\cos(k) + B\cos(2k) - 2\epsilon_a\cos(3k)}{X - e^{ik}W - 2e^{3ik}C + e^{2ik}D + e^{4ik}E}\right|^2, \tag{15}$$

where the coefficients A, B, C, D, E, X, W, and Z are listed in the Appendix.

The resonance condition is now a third-order algebraic equation

$$\begin{aligned} 0 = {} & 8\epsilon_a\cos(k)^3 - 4\epsilon_a(\epsilon_a + 2\epsilon_b)\cos(k)^2 \\ & + \{2\epsilon_b[1 + \epsilon_a(2\epsilon_a + \epsilon_b)] - 6\epsilon_a\}\cos(k) - \epsilon_a^2\epsilon_b^2 \\ & - (\epsilon_a + \epsilon_b)^2 + 2\epsilon_a(\epsilon_a + 2\epsilon_b), \end{aligned} \tag{16}$$

which has three possible real solutions, corresponding to three possible resonances. This equation admits a closed-form solution which is, however, too cumbersome to be of practical use. We resort to the more practical method of solving Eq. (16) numerically and finding the parameter region, in the ϵ_a vs ϵ_b plane, where the resonances (two or three of them) can merge into a single one. To determine that, we set values for ϵ_a and ϵ_b and collect all real solutions k that fulfill the condition $|k_i - k_j| \leqslant 10^{-6}$, where k_i and k_j are real solutions of Eq. (16). When the condition is satisfied, we mark a dot on the ϵ_a,ϵ_b plane. Results from this procedure are shown in Fig. 2. The tetramer curve also ends at finite parameter values: $\epsilon_a = 1.414$, $\epsilon_b = 3.275$. Thus, the curves for the trimer and the tetramer are qualitatively similar, possibly due to the fact that both have a center of symmetry. As mentioned before, when one considers the homogeneous tetramer $\epsilon_a\epsilon_a\epsilon_a\epsilon_a$, all four resonances appear separated from each other and it is not possible to obtain any merging.

C. Pentamer

Now we consider a single segment with $n = 5$ embedded in a linear chain and consider the symmetric site energy distribution $\epsilon_c\epsilon_a\epsilon_b\epsilon_a\epsilon_c$, placed on the sites $n = 0$, 1, 2, 3, and 4 of the chain (see Fig. 1). The transmission and reflection coefficients can be casted in closed form as

$$T = \left|\frac{-1 + e^{2ik}}{(K_1 + e^{ik}A_1 + e^{3ik}B_1 - e^{2ik}C_1)G_1}\right|^2 \tag{17}$$

$$R = \left|\frac{D}{(K_1 + e^{ik}A_1 + e^{3ik}B_1 - e^{2ik}C_1)G_1}\right|^2 \tag{18}$$

where coefficients D, A_1, B_1, C_1, D_1, E_1, F_1, G_1, and K_1 are listed in the Appendix.

The resonance condition ($R = 0$) implies a fourth-order algebraic equation for the wave vector k:

$$\begin{aligned} 0 = {} & 16\epsilon_c\cos(k)^4 + 4\left(-2\epsilon_c^2 - 4\epsilon_c\epsilon_a - 2\epsilon_c\epsilon_b\right)\cos(k)^3 \\ & + \left[4\epsilon_a + 4\epsilon_c^2(2\epsilon_a + \epsilon_b) + 2\epsilon_c\left(-2 + 4\epsilon_a^2 + 8\epsilon_a\epsilon_b\right)\right] \\ & \times \left\{\left[2\epsilon_c^2 - \epsilon_a(\epsilon_a + \epsilon_b) + 2\epsilon_c(2\epsilon_a + \epsilon_b)\right]\cos(k)^2\right. \\ & \left. - \epsilon_c\epsilon_a[\epsilon_a\epsilon_b + \epsilon_c(\epsilon_a + 2\epsilon_b)]\right\}\cos(k) + \epsilon_c^2\epsilon_a^2\epsilon_b \\ & + (2\epsilon_c - 2\epsilon_a + \epsilon_b) + \epsilon_a\left(-2\epsilon_c^2 - 2\epsilon_c\epsilon_b + \epsilon_a\epsilon_b\right). \end{aligned} \tag{19}$$

Thus, we have up to four resonances, which are found by a similar numerical procedure as the one used in Sec. III B for the tetramer. Results are shown in Fig. 3, which shows the curves in the ϵ_a-ϵ_b parameter space, where merging of two resonances is possible, for different values of ϵ_c. As expected, for $\epsilon_c = 0$ (blue line with red circles), which corresponds to the symmetric trimer, the curve coincides quite well with the analytic curve obtained by Giri *et al.* [see Eq. (14)]. By changing the value of ϵ_c we are able to determine other curves

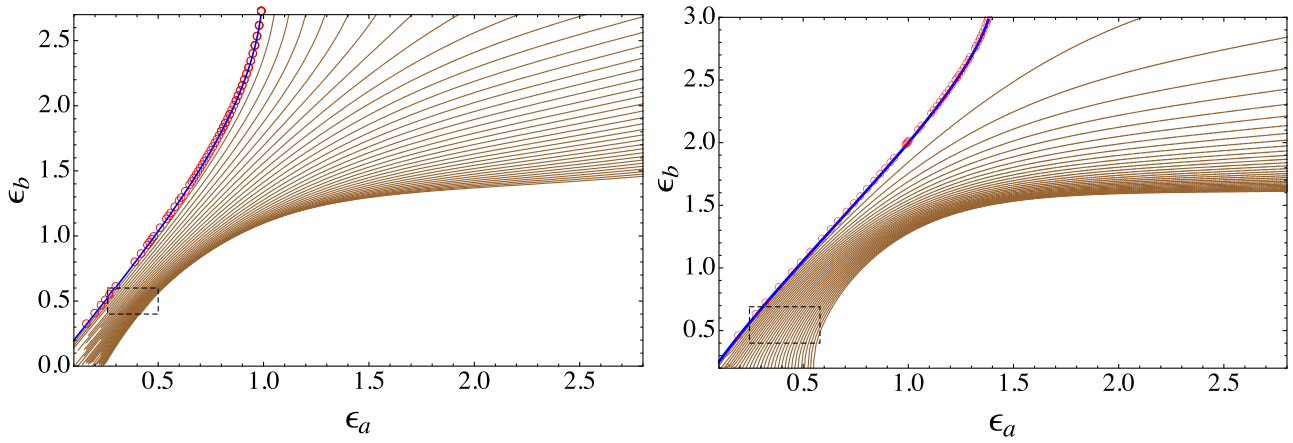

FIG. 3. Parameter region in ϵ_a-ϵ_b plane for the (left) pentamer and (right) hexamer cases, where the merging of two resonances occurs, for different values of ϵ_c. Each curve in brown corresponds to a progressive increase in ϵ_c from $\epsilon_c = 0$ up to $\epsilon_c = 0.31$, in steps of 0.01. The blue curve denotes the case of the symmetric trimer while the red circles correspond to the numerical solution of Eq. (13) for the particular $\epsilon_c = 0$ case.

in the ϵ_a-ϵ_b plane where the tuning is possible. From the figure it seems that, by increasing ϵ_c in progressively smaller steps, a whole allowed region will be obtained where tunability is possible. It should be noted that merging of three or more resonances was not observed.

D. Hexamer

Now we consider a single segment with $n = 6$ embedded in a linear chain, with six site energies distributed symmetrically as $\epsilon_c\epsilon_a\epsilon_b\epsilon_b\epsilon_a\epsilon_c$ (see Fig. 1). As before, we can obtain closed expressions for the transmission and refection coefficients:

$$T = \left|\frac{-1+e^{2ik}}{(-1+e^{ik}H_1)E_2}\right|^2, \tag{20}$$

$$R = \left|\frac{D_3}{(-1+e^{ik}H_1)E_2}\right|^2, \tag{21}$$

where D_3, H_1, and E_2 are defined in the Appendix.

The resonance condition implies a fifth-order algebraic equation,

$$\begin{aligned}0 = {}& \epsilon_c^2 + 2\epsilon_c\epsilon_a - \epsilon_a^2 - \epsilon_c^2\epsilon_a^2 + 2\epsilon_c\epsilon_b - 2\epsilon_a\epsilon_b \\ & - 2\epsilon_c^2\epsilon_a\epsilon_b + \epsilon_b^2 - 2\epsilon_c\epsilon_a\epsilon_b^2 + \epsilon_a^2\epsilon_b^2 + \epsilon_c^2\epsilon_a^2\epsilon_b^2 \\ & - 32\cos(k)^5\epsilon_c + \cos(k)^4\big(16\epsilon_c^2 + 32\epsilon_c\epsilon_a \\ & + 32\epsilon_c\epsilon_b\big) + \cos(k)^3\big(40\epsilon_c - 8\epsilon_a - 16\epsilon_c^2\epsilon_a \\ & - 8\epsilon_c\epsilon_a^2 - 16\epsilon_c^2\epsilon_b - 32\epsilon_c\epsilon_a\epsilon_b - 8\epsilon_c\epsilon_b^2\big) \\ & + \cos(k)^2\big(2\epsilon_c^2 + 4\epsilon_c\epsilon_a + 4\epsilon_a^2 + 4\epsilon_c^2\epsilon_a^2 + 4\epsilon_c\epsilon_b \\ & + 8\epsilon_a\epsilon_b + 16\epsilon_c^2\epsilon_a\epsilon_b + 8\epsilon_c\epsilon_a^2\epsilon_b + 4\epsilon_c^2\epsilon_b^2 + 8\epsilon_c\epsilon_a\epsilon_b^2\big) \\ & + \cos(k)\big(-10\epsilon_c + 6\epsilon_a + 8\epsilon_c^2\epsilon_a + 2\epsilon_c\epsilon_a^2 - 2\epsilon_b \\ & + 4\epsilon_c^2\epsilon_b + 12\epsilon_c\epsilon_a\epsilon_b - 4\epsilon_a^2\epsilon_b - 4\epsilon_c^2\epsilon_a^2\epsilon_b + 4\epsilon_c\epsilon_b^2 \\ & - 2\epsilon_a\epsilon_b^2 - 4\epsilon_c^2\epsilon_a\epsilon_b^2 - 2\epsilon_c\epsilon_a^2\epsilon_b^2\big),\end{aligned} \tag{22}$$

which is solved numerically to find the parameter region where a merging of the resonances occurs. In Fig. 3 we plot the curves in the ϵ_a-ϵ_b plane, for different values of ϵ_c. For $\epsilon_c = 0$ we reobtain the tetramer curve (for appropriate ϵ_a and ϵ_b values). As in the pentamer case, it would seem that, as the sweep in parameter ϵ_c becomes finer and finer, one would obtain a whole continuous region where syntonization of two resonances is possible.

As a conclusion of this section, we could say that,for a given symmetric n-mer, there are at most $n-1$ transmission resonances and that it is possible to engineer a situation where two of them merge, by a judicious choice of the site energies. As the length of the segment is increased past $n = 6$, the number of site energy parameters increases as well, and the determination of the multidimensional resonance region becomes hard to compute. Preliminary computations for some special cases of longer n-mers show results that agree qualitatively with the ones obtained so far. Interestingly enough, the merging of three or more resonances was never observed.

It should be noted that, in all n-mers examined (trimers, tetramers, pentamers, and hexamers) that obey the merging of resonances conditions (see Figs. 2 and 3), the reflection coefficient near the resonance behaves as $O(k-k_c)^4$, where k_c is the resonant wave vector, i.e., where $T = 1$. On the contrary, when the merging condition is not satisfied, we have $n-1$ resonances and around each one the reflection coefficient behaves as $O(k-k_c)^2$, just as in the random dimer model. These facts have profound consequences later, when we consider transport across a disordered array of these n-mers.

IV. RANDOM SYSTEM (MANY n-MER IMPURITIES)

The resonance state guarantees that a single n-mer will be transparent to the transmission of a plane wave at a special wave vector (or energy). It is only natural to wonder whether something of that nature can occur inside a random chain, where the n-mers are placed at random. Obviously, the whole chain will still be transparent at the resonant wave vector for the single n-mer, but we wonder what happens for a general excitation containing many wave vectors. At first it would seem that Anderson localization would impede the transmission of plane waves or the diffusion of a localized excitation. However,

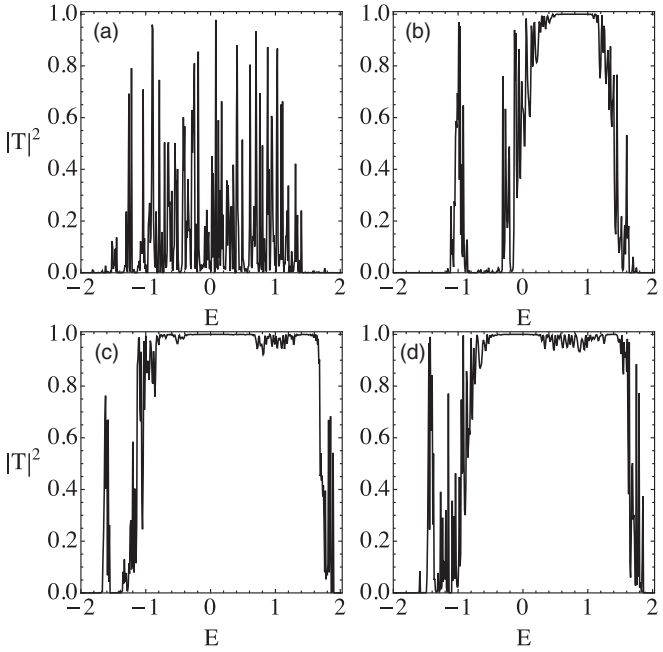

FIG. 4. Transmission coefficient $|T|^2$ as a function of the energy E for a single-realization disordered region of size $L = 400$ containing randomly placed (a) single impurities and (b)–(d) pentamer impurities, at %50 concentration: (a) $\epsilon_n \in [-0.25,0.25]$; (b) $\epsilon_c = 0$, $\epsilon_a = 0.27$, $\epsilon_b = 0.545$ (symmetric trimer); (c) $\epsilon_c = 0.1$, $\epsilon_a = 0.34$, $\epsilon_b = 0.465$; and (d) $\epsilon_c = 0.23$, $\epsilon_a = 0.45$, $\epsilon_b = 0.511$.

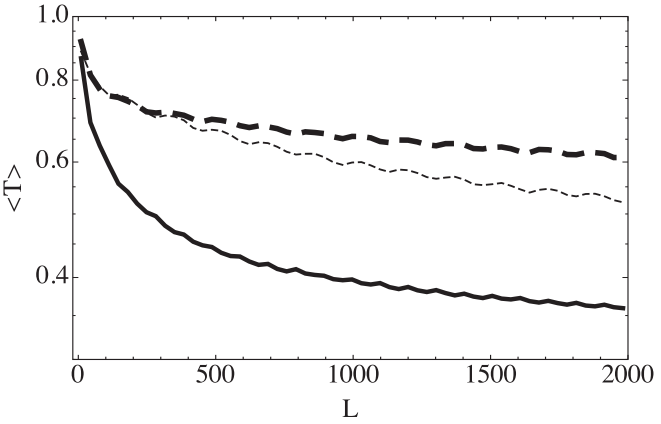

FIG. 5. Averaged transmission vs disordered length for some representative pentamer cases. The thick dashed curve corresponds to $\epsilon_c = 0.1$, $\epsilon_a = 0.34$, and $\epsilon_b = 0.465$. The thin dashed line corresponds to $\epsilon_c = 0.23$, $\epsilon_a = 0.45$, and $\epsilon_b = 0.511$. The continuous line corresponds to $\epsilon_c = 0$, $\epsilon_a = 0.27$, and $\epsilon_b = 0.545$ (symmetric trimer). All these values fall inside the rectangular region marked in Fig. 3. Note the logarithmic scale on the vertical axis.

it was found that, for the random dimer model [7] and the random trimer model [8], that around each resonance, there is a small region containing states whose localization length is of the order of the size of the system or larger. Thus, the system allows the passage of an incoming wave whose energy is close to the resonance energy or energies.

In this section we examine numerical results for the transmission coefficients focusing on the pentamer ($n = 5$) case. The behavior for the others n-mers is qualitatively similar and is not shown for the sake of brevity. We consider three site energy cases, for each one. Figure 4 shows the transmission coefficient (for a single disorder realization) in the absence of nonlinearity ($\chi = 0$), vs the energy [$E = 2\cos(k)$] for some parameter values where it was possible to merge two of the resonances discussed in the previous section. Figure 4(a) corresponds to the pure Anderson case, with single impurities randomly placed, with $\epsilon_n \in [-0.25,0.25]$. Figure 4(b) corresponds to $\epsilon_c = 0$, $\epsilon_a = 0.27$, $\epsilon_b = 0.545$. This configuration is nothing else but the symmetric trimer. Next we have the *bona fide* pentamer cases of Fig. 4(c) with $\epsilon_c = 0.1$, $\epsilon_a = 0.34$, and $\epsilon_b = 0.465$, and Fig. 4(d) with $\epsilon_c = 0.23$, $\epsilon_a = 0.45$, and $\epsilon_b = 0.511$. These three cases are contained in the parameter region inside the rectangle shown in Fig. 3. Clearly, an increment in the width of the plane-wave transmission is observed, in comparison with the standard Anderson case, shown in Fig. 4(a). This behavior was also observed for all the other n-mers (not shown).

Thus, in the presence of disorder, and inside the resonance regime, the transmission coefficient across a disordered chain displays higher transmission values than in the pure Anderson case, as expected.

A. Linear transmission as a function of system length

In the absence of correlations, Anderson localization dominates and in this case it is well known that the transmission coefficient decreases exponentially with the size of the system [13]. In the presence of short-range correlations, this image changes, as we will see.

Let us now consider the transmission coefficient of plane waves through a chain segment of length L, characterized by a site energy distribution $\{\epsilon_n\}$ and zero nonlinearity $\chi = 0$, that is joined on both sides to semi-infinite linear homogeneous chains, characterized by having $\epsilon_n = 0 = \chi$. The segment contains a fraction (50%) of identical pentamer ($n = 5$) defects, randomly distributed. The site energy values $\{\epsilon_n\}$ are taken as obeying the pentamer resonance condition, Eq. (19).

To compute numerically the transmission coefficient as a function of length, we use Eq. (6), then Eq. (7), followed by a double average over 200 disorder realizations and over all wave vectors. In this manner we obtain a global estimate about the transmissivity of the disordered chain. Results are shown in Fig. 5. We see that the transmission decreases slower than exponential and behaves as a power law: $\langle T \rangle \sim aL^{-b}$. The values of a and b depend on the actual value of the $\{\epsilon_n\}$.

A measure of the spatial extension of an eigenstate of our system with correlated disorder is given by the participation ratio (PR), defined as [14]

$$\mathrm{PR} = \frac{\left(\sum_i^N |c_i|^2\right)^2}{N\left(\sum_i^N |c_i|^4\right)}, \tag{23}$$

where N is the size of the system. For a completely localized state, $\mathrm{PR} = O(1/N)$, while for an extended state, $\mathrm{PR} = O(1)$.

In Fig. 6 we show the results of the computation of the PR for three representative pentamer cases. Each point on Fig. 6 corresponds to the PR value at that energy and for a particular

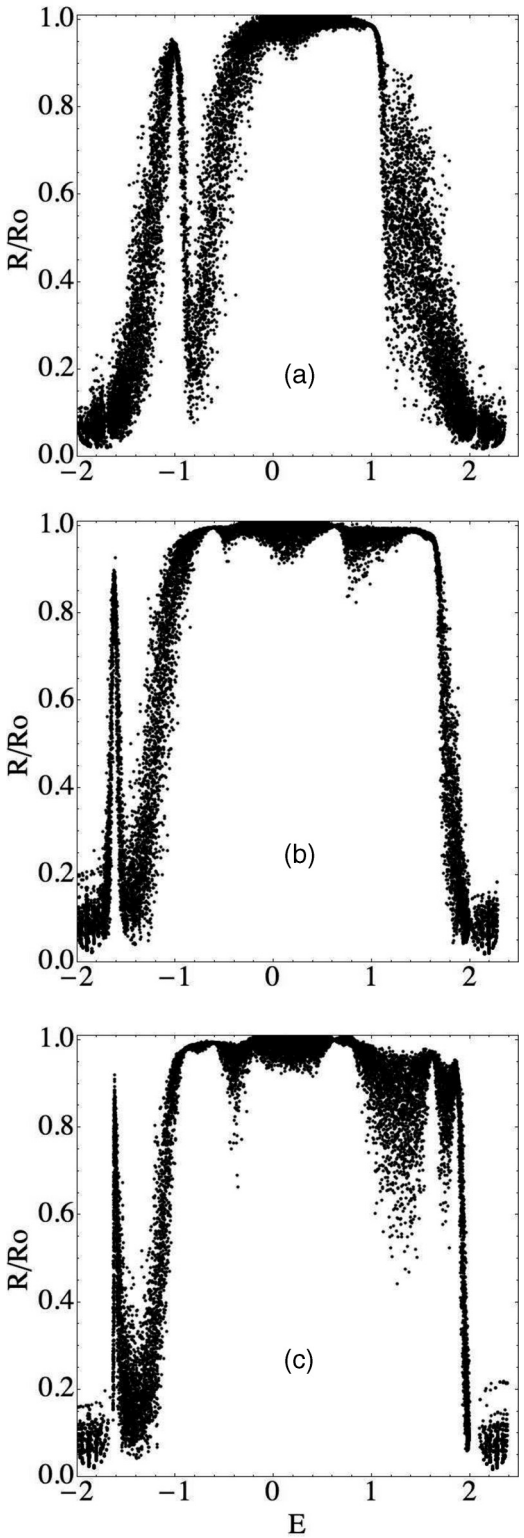

FIG. 6. Participation ratio as a function of energy for a number of random realizations, for a chain of size $L = 400$, containing 50% of pentamer impurities: (a) $\epsilon_c = 0$, $\epsilon_a = 0.27$, and $\epsilon_b = 0.545$ (symmetric trimer); (b) $\epsilon_c = 0.1$, $\epsilon_a = 0.34$, and $\epsilon_b = 0.465$; and (c) $\epsilon_c = 0.23$, $\epsilon_a = 0.45$, and $\epsilon_b = 0.511$.

disorder realization. In total, 50 realizations were used for a chain of 400 sites.

We note a clear difference in the amount of states effectively extended that exist between the case of the symmetric trimer [Fig. 6(a)] and the pentamer cases [Figs. 6(b) and 6(c)]. In the latter, the width of the resonance is greater (see Fig. 4), leading to a greater number of wave vectors with a mean free path of the order of the system length, implying a greater transmission coefficient, that is, a smaller decay of the transmission with system size. Also we notice the presence of secondary peaks in Figs. 6(a)–6(c). They cannot be attributed to standard Azbel resonances [15] since the width of these scale as $e^{-2L/\xi}$. Taking $\xi \sim 100$ and $L = 400$, we obtain a width of $O(10^{-4})$. One might conjecture that the presence of correlation in the disorder might give rise to an enhanced degeneracy of the states as well as a greater localization length. These two ingredients together could produce and enhance Azbel resonance. The specific width seems to depend on the details of the site energies inside the n-mer.

As can be appreciated from Figs. 5 and 6 and from the effective width of the extended states shown in Figs. 4, 5, and 6 near the resonance energies of the system, there is a higher probability for transmission of plane waves for the symmetric pentamer (and hexamer) case in comparison to the symmetric trimer case.

B. Nonlinear transmission as a function of system length

Let us now consider a chain segment of length L, characterized by a site energy distribution $\{\epsilon_n\}$ and a nonlinear coefficient χ, that is joined on both sides to semi-infinite linear homogeneous chains, characterized by having $\epsilon_n = 0 = \chi$. The segment contains a fraction (50%) of identical pentamer ($n = 5$) defects, randomly distributed. We want to compute the transmission coefficient of plane waves as a function of the length of the segment. As in the linear case, the site energy values $\{\epsilon_n\}$ are taken as obeying the pentamer resonance condition, Eq. (19).

In the presence of nonlinearity we use Eq. (2):

$$EC_n + (\epsilon_n + \chi|C_n|^2)C_n + V(C_{n+1} + C_{n-1}) = 0. \quad (24)$$

Now, in general when one considers the propagation of a plane wave across a disordered linear segment, the transmission coefficient will be a function of the incident wave vector only, for a fixed segment length and underlying disorder. The picture changes, however, if one considers a nonlinear segment. Now, the transmission coefficient depends also on the amplitude of the incoming wave. If one sets up the computation of the transmission in the usual manner, one finds that there is no single output for a given input; i.e., there is multistability [16]. A way to circumvent this and obtain an estimate for the effective transmission is to work in reverse: For a given k, χ and a disordered realization of the segment, one fixes the output amplitude, then iterates backwards until reaching the initial site of the segment, and computes the transmissivity as the ratio of the (fixed) output to the input. Figure 7 shows the average transmission of plane waves through a nonlinear disordered segment as a function of the segment length, for a fixed $\chi = 1$, for the pentamer case. For the hexamer case (not shown) the plot is similar. Also, and according to the results from Sec. II, this plot is equivalent to the one where the output transmission T is kept constant while χ is varied (not shown).

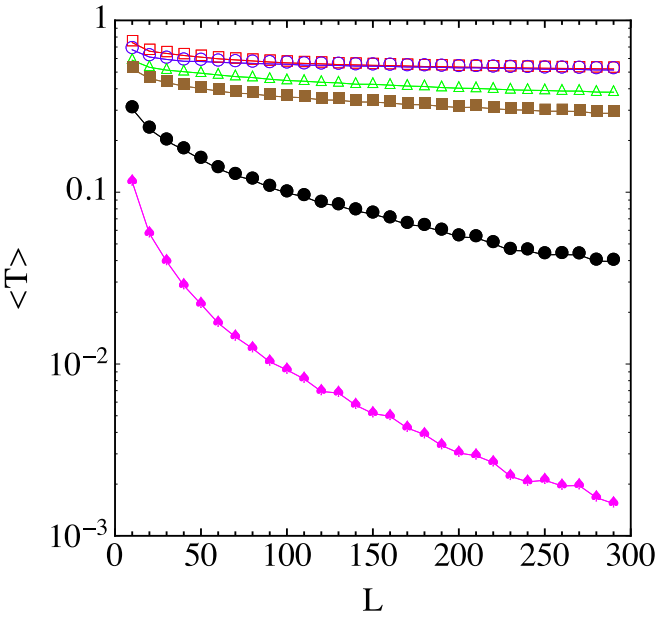

FIG. 7. Average transmission of plane waves through a nonlinear disordered segment as a function of the segment length. Left: We fix $\chi = 1$ and vary the output transmission from top to bottom as $T = 0.1, 0.3, 0.5, 0.6, 0.8$, and 1.0.

One way of visualizing the transmissivity of a given segment is to use a single disorder realization and a given wave vector k and nonlinear coefficient χ, and to compute the transmission. If this is greater than an arbitrary critical amount, the wave is said to be "passing," and a black dot is marked in the χ vs k plane; otherwise it is "nonpassing," and no marking is done. Typically, the critical amount separating the "passing" from the "nonpassing" regime is of the order $\exp(L)$, where L is the length of the segment. Figure 8 shows results of this procedure carried out for a segment containing pentamer impurities. We note the irregular, fractal-like shape, featuring the presence of several branches, due to multistability [16,17]. In Table I, we show the fractal dimensions of the transmission diagrams, computed by the method of box counting. These fractal transmission shapes look quite similar to the ones obtained for the case of Anderson disorder on a nonlinear background [18]. At small nonlinearities, most of the waves can pass, but their number decreases as nonlinearity is increased, until some maximum value of χ is reached where all the waves are nonpassing. Near the boundaries of the passing-nonpassing regions there is extreme sensitivity in transmission with χ and k. In Fig. 9 we plot the results for the fitted averaged transmittance as a function of segment length L for pentamer and trimer cases, and for a couple of nonlinearity values, taking 100 disorder realizations and averaging over all wave vectors in $0 \leqslant k \leqslant \pi$. As anticipated from Figs. 4 and 5 we see that, for a given segment length

TABLE I. Fractal dimension for each transmission diagram of Fig. 8.

Configuration	Fractal dimension
(a)	1.703
(b)	1.785
(c)	1.777

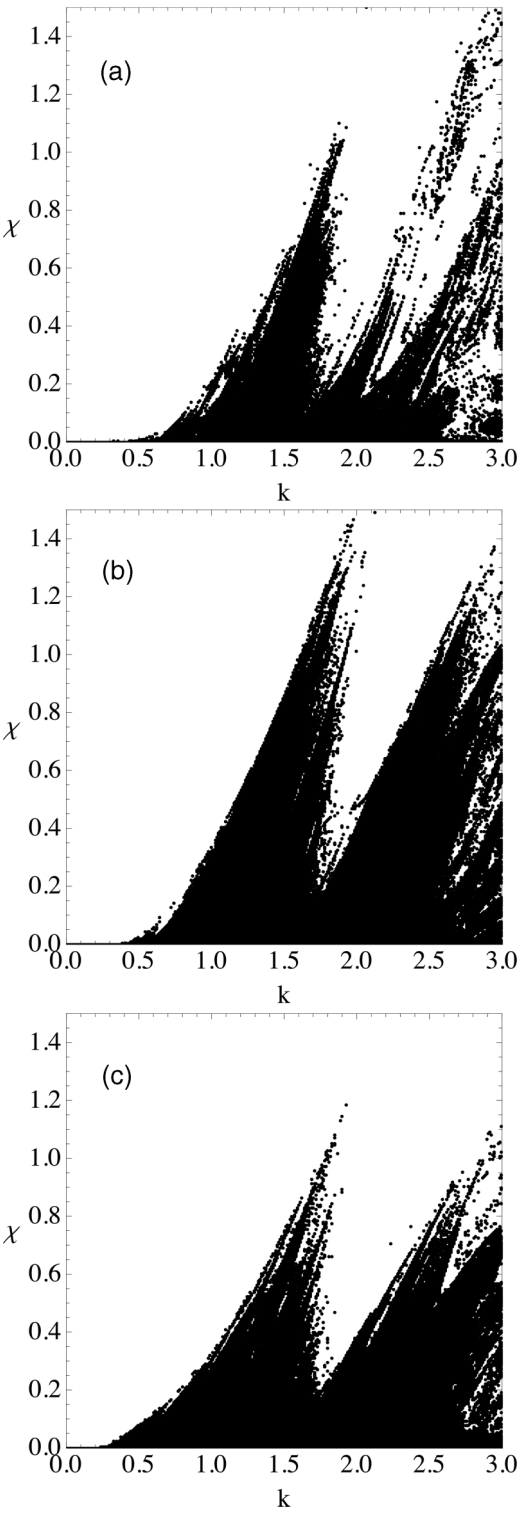

FIG. 8. Transmitting (black) and nontransmitting (white) regions for a symmetric pentamer with $L = 400$ for (a) $\epsilon_c = 0.1$, $\epsilon_a = 0.34$, and $\epsilon_b = 0.465$; (b) $\epsilon_c = 0.23$, $\epsilon_a = 0.45$, and $\epsilon_b = 0.511$; and (c) $\epsilon_c = 0$, $\epsilon_a = 0.27$, and $\epsilon_b = 0.545$.

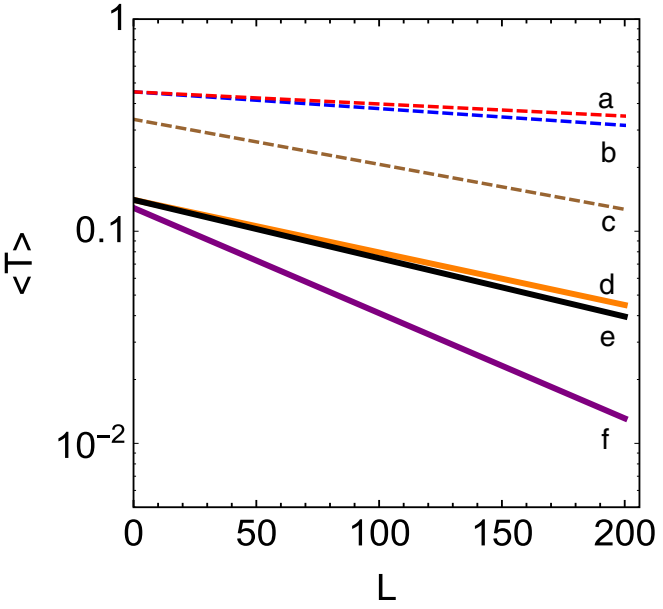

FIG. 9. Fitted average transmittance $\langle T\rangle \sim \exp(-b(\chi)L)$ as a function of segment length in the nonlinear regime and for $L = 200$ and averaged over 100 disorder realizations for three n-mer cases. Dashed curves are for $\chi = 0.3$ and continuous lines are for $\chi = 0.7$. (a) Pentamer with $\epsilon_c = 0.1$, $\epsilon_a = 0.34$, and $\epsilon_b = 0.465$, with fitting function $b(\chi) = 0.068 + 0.55\chi + 11.99\chi^2$; (b) pentamer with $\epsilon_c = 0.23$, $\epsilon_a = 0.45$, and $\epsilon_b = 0.511$, with fitting function $b(\chi) = 0.108 + 3.97\chi + 5.74\chi^2$; (c) trimer with $\epsilon_c = 0.0$, $\epsilon_a = 0.27$, and $\epsilon_b = 0.545$, with fitting function $b(\chi) = -0.270 + 17.53\chi - 1.19\chi^2$; (d) pentamer with $\epsilon_c = 0.1$, $\epsilon_a = 0.34$, and $\epsilon_b = 0.465$, with fitting function $b(\chi) = 0.068 + 0.55\chi + 11.99\chi^2$; (e) pentamer with $\epsilon_c = 0.23$, $\epsilon_a = 0.45$, and $\epsilon_b = 0.511$, with fitting function $b(\chi) = 0.108 + 3.97\chi + 5.74\chi^2$; and (f) trimer with $\epsilon_c = 0.0$, $\epsilon_a = 0.27$, and $\epsilon_b = 0.545$, with fitting function $b(\chi) = -0.270 + 17.53\chi - 1.19\chi^2$. In all cases the statistical coefficient of determination is around 0.99. Note the semilogarithmic scale.

L, the average transmission is greater for a pentamer than for the trimer case. This tendency of higher transmission with the length of the n-mer seems to quickly reach a saturation. For the hexamer, the transmission curves are already very close to the ones for the pentamer. For segment lengths $0 < L < 200$ the transmittance curves behave as $\langle T\rangle \sim \exp(-b(\chi)L)$ to a good accuracy, where $b(\chi)$ is an increasing function of χ. Figure 10 is similar to Fig. 9, except for much longer segment lengths. In this case the curves seem to decay more slowly than for short segments. More specifically, the behavior is now of the form $\langle T\rangle \sim L^{-\gamma(\chi)}$ to a good accuracy, where $\gamma(\chi)$ is again an increasing function of χ. A simple quadratic fit for both, $b(\chi)$ and $\gamma(\chi)$ result in a high goodness of fit, with a determination coefficient very close to unity: ∼0.99 [19].

As a conclusion of this section, we can say that the presence of nonlinearity tends to inhibit the propagation of extended excitations. Also (not shown), the propagation does not depend qualitatively on the type of n-mer used or whether the $\{\epsilon_n\}$ values satisfy the merging of resonances condition. As we see next, these results are in marked contrast with the results for the localized excitation.

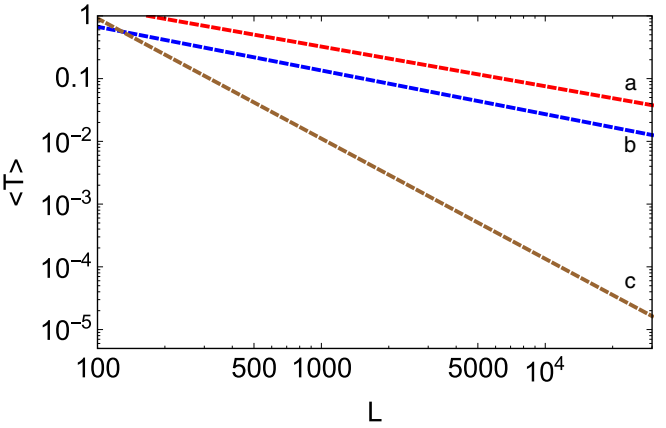

FIG. 10. Fitted average transmittance $\langle T\rangle \sim L^{-\gamma(\chi)}$ as a function of segment length in the nonlinear regime ($\chi = 0.3$) and for $L = 30\,000$ and averaged over 100 disorder realizations for three n-mer cases: (a) pentamer with $\epsilon_c = 0.1$, $\epsilon_a = 0.34$, and $\epsilon_b = 0.465$, with fitting function $\gamma(\chi) = 0.421 - 0.228\chi + 3.102\chi^2$; (b) pentamer with $\epsilon_c = 0.23$, $\epsilon_a = 0.45$, and $\epsilon_b = 0.511$, with fitting function $\gamma(\chi) = 0.575 - 1.651\chi + 6.85\chi^2$; and (c) trimer with $\epsilon_c = 0.0$, $\epsilon_a = 0.27$, and $\epsilon_b = 0.545$, with fitting function $\gamma(\chi) = 0.718 - 0.86\chi + 16.202\chi^2$. In all cases the statistical coefficient of determination is around 0.99. Note the log-log scale.

V. PROPAGATION OF LOCALIZED EXCITATIONS IN THE LINEAR AND NONLINEAR REGIMES

Having examined in the previous section the propagation characteristics of an extended excitation across a nonlinear medium populated with n-mers randomly placed, we now consider the propagation of an excitation, which is initially placed completely on a single site ($n = n_0$) inside the disordered and nonlinear medium. For a fixed value of χ and a given random configuration of n-mers, we compute the behavior of its mean square displacement (MSD) as a function of "time" z,

$$u(z) = \frac{\sum_{n=-\infty}^{\infty}(n-n_0)^2|C_n(z)|^2}{\sum_{n=-\infty}^{\infty}|C_n(z)|^2}, \tag{25}$$

followed by an average over a number of disordered realizations, obtaining $\langle u(z)\rangle$. The system of equations (1) is solved numerically with a fourth-order Runge-Kutta algorithm. Numerical precision is checked by monitoring the conservation of the norm $\sum_n |C_n|^2$. Also, and in order to avoid deleterious boundary effects, we use a self-expanding lattice [20]. At long propagation distances, one expects the MSD to behave as $\langle u(z)\rangle \sim z^\alpha$, where $\alpha = 2$ is a ballistic propagation, while $\alpha < 1 (\alpha > 1)$ denotes subdiffusive (superdiffusive) propagation.

Results are shown in Fig. 11 for three pentamer cases, where for ease in visualization we have plotted $\langle u(z)\rangle/z^\alpha$, where α is the exponent in the absence of nonlinearity. Notably, we find that only five disorder realizations are needed to obtain $\langle u(z)\rangle$ to a good precision. Increasing the number of realizations does not lead to any significant change. The behavior is of the form $\langle u(z)\rangle \sim z^\alpha$ with $\alpha \sim 1.8$, regardless of nonlinearity, but seems to depend weakly on the site energies $\{\epsilon_a,\epsilon_b,\epsilon_c\}$.

Note that the vertical axis of each plot is different since we are plotting $\langle u(z)\rangle/z^\alpha$ vs z. For the first plot [Fig. 11(a)], $\alpha = 1.81$, and we notice that an increase in nonlinearity does

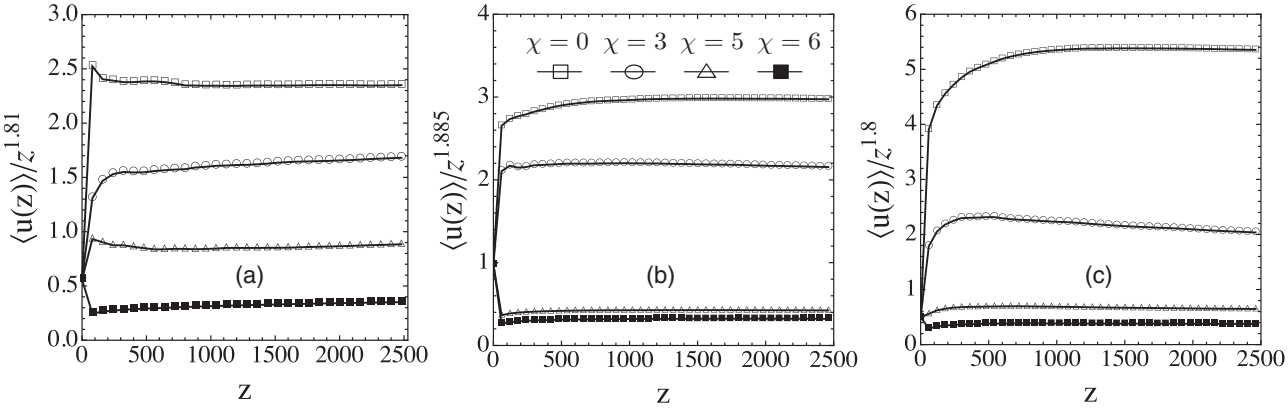

FIG. 11. MSD for three pentamer cases: (a) $\epsilon_c = 0.0$, $\epsilon_a = 0.27$, and $\epsilon_b = 0.545$ (symmetric trimer); (b) $\epsilon_c = 0.1$, $\epsilon_a = 0.34$, and $\epsilon_b = 0.465$; and (c) $\epsilon_c = 0.23$, $\epsilon_a = 0.45$, and $\epsilon_b = 0.511$, all taken from inside the region marked with a rectangle in Fig. 3.

not change the exponent, but decreases the "speed" of the propagation. Next, in Fig. 11(b), $\alpha = 1.885$. This value was checked by running the computation up to $z_{\max} = 10^4$. Here too, as in Fig. 11(a), an increase in nonlinearity does not change the asymptotic exponent for the MSD, but it does decrease the propagation speed. Finally, in Fig. 11(c), we repeat what we did in Fig. 11(b) for a different parameter set and this time $\alpha = 1.8$, almost the same as in Fig. 11(a). As before, an increase in nonlinearity reduces the speed of propagation but not the exponent. It should be emphasized that the site energy values were taken from Fig. 3 and, thus, satisfy the merging of resonances condition discussed in Sec. III. It should also be mentioned that the same results are obtained for the other n-mers (tetramers and hexamers).

The asymptotic independence of the MSD with nonlinearity can be explained as follows: As the wave propagates inside the segment, its amplitude decreases because of conservation of the norm. This causes a decrease of $|C_n(z)|^2$ and, therefore, of the nonlinear term $\chi|C_n(z)|^2$ with the result that, at long enough propagation distance z, its effect will be negligible. That is why the propagation exponent is independent of χ. Also, the effect of a decrease in the speed of the MSD with an increase of χ can be attributed to the tendency of nonlinearity to trap the wave in the vicinity of the initial site. The portion of the wave that can propagate is smaller, and renormalizes $\langle u(z)\rangle$ to smaller values, but without affecting the propagation exponent [18].

What happens to the exponents when the $\{\epsilon_i\}$ do not fall on the resonance curves of Fig. 3, but instead they are arbitrary? For simplicity, let us focus on the linear case ($\chi = 0$). In this case, as we can see from Fig. 12, as soon as the $\{\epsilon_i\}$ do not fulfill the resonance condition but are kept at relatively small values, the transmission exponent becomes $\alpha = 1.5$ which is characteristic of the random dimer model. This is to be expected since in this case there are only isolated resonances, each of which brings us back to the random dimer phenomenology. Also, when the contrast between the $\{\epsilon_i\}$ is large, Anderson localization sets in, as Fig. 13 shows. This is also in agreement with the random dimer phenomenology.

As a conclusion of this section, we can say that the asymptotic exponent for the MSD of a localized excitation

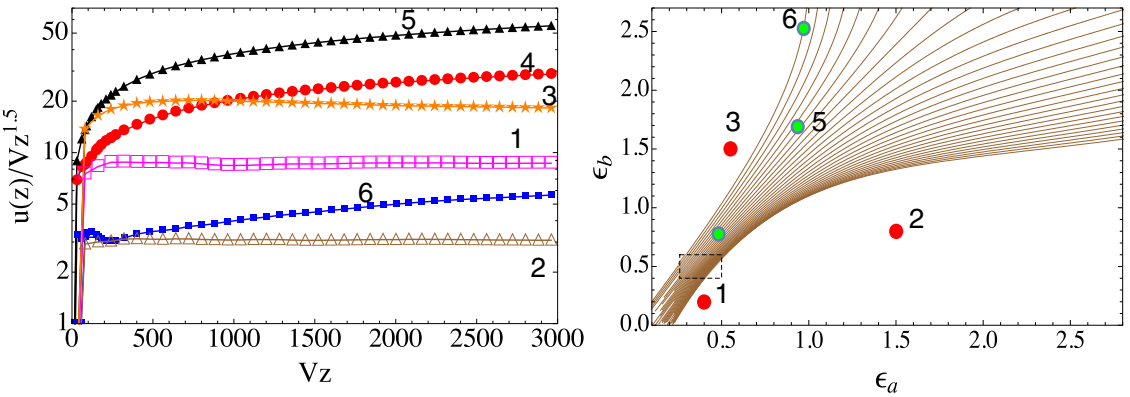

FIG. 12. Left: MSD $u(t)/vz^{1.5}$ vs Vz for different values of the site energies $\{\epsilon_i\}$ for the pentamer case. Curves 1, 2, and 3, marked as red dots on the right-hand side of the figure, correspond to cases that lie outside the resonance condition, while curves 4, 5, and 6, marked as green dots on the right-hand side, fulfill the resonance condition. The values of the site energies are (1) $\epsilon_c = 0.01$, $\epsilon_b = 0.55$, and $\epsilon_a = 1.5$; (2) $\epsilon_c = 0.2$, $\epsilon_b = 0.4$, and $\epsilon_a = 0.2$; (3) $\epsilon_c = 0.3$, $\epsilon_b = 1.5$, and $\epsilon_a = 0.8$; (4) $\epsilon_c = 0.05$, $\epsilon_b = 0.48$, and $\epsilon_a = 0.775$; (5) $\epsilon_c = 0.05$, $\epsilon_b = 0.94$, and $\epsilon_a = 1.69$; and (6) $\epsilon_c = 0.0$, $\epsilon_b = 0.97$, and $\epsilon_a = 2.53$.

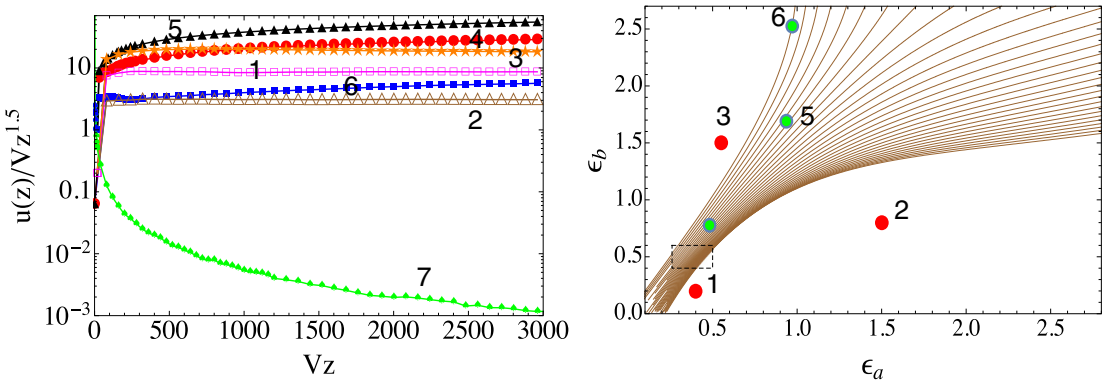

FIG. 13. Same as in Fig. 12, but this time including a new case: $\epsilon_c = 0.0$, $\epsilon_b = 0.5$, and $\epsilon_a = 7$, marked as curve 7.

does not depend on nonlinearity, which merely decreases the speed of propagation due to trapping effects. However, the exponent does depend strongly on whether the site energies inside the n-mers fulfill the resonance condition.

VI. DISCUSSION

We have examined the transport of extended and localized excitations across one-dimensional linear chains embedded with identical linear and nonlinear symmetric n-mers (trimers, tetramers, pentamers, and hexamers), randomly distributed, with a 50% concentration. First, we computed the transmission coefficient of plane waves across a single n-mer, in closed form (from the trimer up to the hexamer), which showed $n-1$ resonances. We attempted to obtain the values of the site energies needed for two or more resonances to merge. This merging is important since it determines the number of states with a localization length greater than or equal to the system length. However, we found that, at most, only two resonances could be merged, implying that the propagation characteristics of an initially localized excitation for all n-mers would be similar to the one present in the previously studied linear symmetric trimer. This turned out to be the case.

Concerning the transmission of plane waves across a segment populated with nonlinear n-mers randomly placed in the linear chain, we found that the behavior of all n-mers was quite similar and, thus, we showed explicit results for the pentamer ($n = 5$) case only. It should be emphasized that, for all n-mers, the values of all site energies were chosen to fulfill the resonance merging condition. We observed that the presence of nonlinearity tended to inhibit the propagation of extended excitations, regardless of the $\{\epsilon_n\}$ values and segment length. But we also observed that this result did not change if the values of the site energies inside the n-mer did not satisfy the merging-of-resonances condition. For short chains the transmissivity decayed exponentially with the segment length; for long segments the transmissivity decayed as a power law, with an exponent that increased with nonlinearity. For the case of the diffusion of an initially localized excitation inside the disordered and nonlinear segment, we found that the asymptotic exponent for its MSD is nearly the same for all n-mers, remaining close to the trimer value $\sim z^{1.8}$. It seems to depend weakly on the values of the site energies inside the n-mer, but it does not depend on nonlinearity, which merely decreases the speed of propagation due to trapping effects. The exponent does, however, depend strongly on whether the site energies inside the n-mer fulfill the resonance condition. When the resonance condition is not satisfied, the exponent reverts back to the random dimer model exponent, $\sim z^{1.5}$. This behavior is not hard to understand since when two resonances are not merged, the curvature of each one around its respective resonance is quadratic in the wave vector, the same as in the random dimer model, thus leading to the same propagation exponent. When two resonances are merged, the curvature of the transmission curve becomes quartic in the wave vector, leading to a similar exponent as in the symmetric trimer case, $\alpha \sim 1.8$. It would seem that the fact that for all n-mers only two resonances could be made to merge is responsible for the rather similar transport properties of extended and localized excitations for all n-mers.

ACKNOWLEDGMENTS

This work was partially supported by FONDECYT Grant No. 1120123, Programa ICM P10-030-F, Programa de Financiamiento Basal de CONICYT (Grant No. FB0824/2008). D.L. acknowledges partial support from a CONICYT Fellowship (Grant No. BCH6852/2013). The authors are grateful to R. Vicencio for useful discussions.

APPENDIX: COEFFICIENTS FOR THE TRANSMISSION THROUGH VARIOUS SINGLE n-MERS

1. Trimer [Eq. (11)]

$$A = 2\epsilon_a(\epsilon_a + \epsilon_b),$$
$$B = (2\epsilon_a + \epsilon_b),$$
$$C = \epsilon_a(\epsilon_a + e^{2ik}\epsilon_a + 2\epsilon_b). \quad \text{(A1)}$$

2. Tetramer [Eq. (15)]

$$
\begin{aligned}
A &= 2\epsilon_b[1+\epsilon_a(2\epsilon_a+\epsilon_b)],\\
B &= 2\epsilon_a(\epsilon_a+2\epsilon_b),\\
C &= \epsilon_a\epsilon_b(\epsilon_a+\epsilon_b),\\
D &= \left(-1+\epsilon_a^2+4\epsilon_a\epsilon_b+\epsilon_b^2\right),\\
E &= \epsilon_a\left(\epsilon_a+2\epsilon_b+\epsilon_a\epsilon_b^2\right),\\
X &= 1+e^{6ik}\epsilon_a^2-2e^{5ik}\epsilon_a^2\epsilon_b,\\
W &= 2(\epsilon_a+\epsilon_b),\\
Z &= \epsilon_a^2+2\epsilon_a\epsilon_b+\left(1+\epsilon_a^2\right)\epsilon_b^2.
\end{aligned}
\tag{A2}
$$

3. Pentamer [Eq. (17)]

$$
\begin{aligned}
D = {} & F_1 - E_1\cos(k) + D_1\cos(2k) - X_1\cos(3k)\\
& + 2\epsilon_c\cos(4k),
\end{aligned}
\tag{A3}
$$

where

$$
\begin{aligned}
A_1 &= \epsilon_c+\epsilon_a+\epsilon_b,\\
B_1 &= \epsilon_a(1+\epsilon_c\epsilon_b),\\
C_1 &= -1+\epsilon_a\epsilon_b+\epsilon_c(\epsilon_a\ +\epsilon_b),\\
D_1 &= 2\{\epsilon_a[1+\epsilon_c(2\epsilon_c+\epsilon_a)]\\
&\quad +\epsilon_c(\epsilon_c+2\epsilon_a)\epsilon_b\},\\
E_1 &= 2\left\{\epsilon_a(\epsilon_a+\epsilon_b)+\epsilon_c^2\left(1+\ \epsilon_a^2+2\epsilon_a\epsilon_b\right)\right.\\
&\quad \left.+\epsilon_c[\epsilon_b+\ \epsilon_a(2+\epsilon_a\epsilon_b)]\right\},\\
F_1 &= 2\epsilon_c\epsilon_a(\epsilon_c+\epsilon_a)+\left[1+2\epsilon_c\epsilon_a\right.\\
&\quad \left.+\epsilon_a^2+\epsilon_c^2\left(2+\epsilon_a^2\right)\right]\epsilon_b
\end{aligned}
$$

$$
\begin{aligned}
G_1 &= 1-e^{ik}\epsilon_a+e^{2ik}\epsilon_c(\epsilon_a-2\cos k),\\
K_1 &= -1+e^{5ik}\epsilon_c-e^{4ik}\epsilon_c(\epsilon_a+\epsilon_b),\\
X_1 &= 2\epsilon_c(\epsilon_c+2\epsilon_a+\epsilon_b).
\end{aligned}
\tag{A4}
$$

4. Hexamer [Eq. (24)]

$$
\begin{aligned}
D_3 = {} & \{A_2 - 2B_2\cos(k) + 2C_2\cos(2k)\\
& - 2D_2\cos(3k) + 2\epsilon_c[\epsilon_c+2(\epsilon_a+\epsilon_b)]\cos(4k)\\
& - 2\epsilon_c\cos(5k)\},\\
H_1 = {} & -1+\epsilon_b+e^{ik}\epsilon_a[1-\epsilon_b+2\cos(k)]\\
& + e^{2ik}\epsilon_c F_2,
\end{aligned}
\tag{A5}
$$

where

$$
\begin{aligned}
A_2 &= \epsilon_a^2+2\epsilon_a\epsilon_b+\left(1+\epsilon_a^2\right)\epsilon_b^2+\epsilon_c^2\left[1+\epsilon_a^2+6\epsilon_a\epsilon_b\right.\\
&\quad \left.+\left(2+\epsilon_a^2\right)\epsilon_b^2\right]+2\epsilon_c[\epsilon_b+\epsilon_a(1+2\epsilon_a\epsilon_b+\epsilon_b^2)],\\
B_2 &= 2\epsilon_c\epsilon_a(\epsilon_c+\epsilon_a)+\epsilon_b+2\left[3\epsilon_c\epsilon_a+\epsilon_a^2\right.\\
&\quad \left.+\epsilon_c^2\left(2+\epsilon_a^2\right)\right]\epsilon_b+\left[\epsilon_a+\epsilon_c\left(1+2\epsilon_c\epsilon_a+\epsilon_a^2\right)\right]\epsilon_b^2,\\
C_2 &= \epsilon_a(\epsilon_a+2\epsilon_b)+2\epsilon_c(\epsilon_a+\epsilon_b)(1+\epsilon_a\epsilon_b)\\
&\quad +\epsilon_c^2\left(1+\epsilon_a^2+4\epsilon_a\epsilon_b+\epsilon_b^2\right),\\
D_2 &= \epsilon_c\epsilon_a^2+\epsilon_c\epsilon_b(2\epsilon_c+\epsilon_b)+\epsilon_a[1+2\epsilon_c(\epsilon_c+2\epsilon_b)],\\
E_2 &= -1+e^{ik}\{1+\epsilon_b-e^{ik}\epsilon_a[1+\epsilon_b-2\cos(k)]\\
&\quad +e^{2ik}\epsilon_c[1+\epsilon_a+\epsilon_a\,\epsilon_b-2(1+\epsilon_a+\epsilon_b)\\
&\quad \times\cos(k)+2\cos(2k)]\},\\
F_2 &= (1+\epsilon_a(-1+\epsilon_b)-2(-1+\epsilon_a+\epsilon_b)\cos(k)\\
&\quad +2\cos(2k)).
\end{aligned}
\tag{A6}
$$

[1] P. W. Anderson, Phys. Rev. **109**, 1492 (1958).

[2] B. Kramer and A. MacKinnon, Rep. Prog. Phys. **56**, 1469 (1993); E. Abrahams, *50 Years of Anderson Localization* (World Scientific, Singapore, 2010).

[3] D. N. Christodoulides, F. Lederer, and Y. Silberberg, Nature (London) **424**, 817 (2003).

[4] Y. Lahini, A. Avidan, F. Pozzi, M. Sorel, R. Morandotti, D. N. Christodoulides, and Y. Silberberg, Phys. Rev. Lett. **100**, 013906 (2008).

[5] M. Segev, Y. Silberberg, and D. N. Christodoulides, Nat. Photonics **7**, 197 (2013).

[6] J. C. Flores, J. Phys.: Condens. Matter **1**, 8471 (1989).

[7] D. H. Dunlap, H. L. Wu, and P. W. Phillips, Phys. Rev. Lett. **65**, 88 (1990).

[8] D. Giri, P. K. Datta, and K. Kundu, Phys. Rev. B **48**, 14113 (1993).

[9] U. Naether, S. Stützer, R. Vicencio, M. I. Molina, A. Tünnermann, S. Nolte, T. Kottos, D. N. Christodoulides, and A. Szameit, New J. Phys. **15**, 013045 (2013).

[10] R. Farchioni and G. Grosso, Phys. Rev. B **56**, 1170 (1997).

[11] S. N. Evangelou and E. N. Economou, J. Phys. A **26**, 2803 (1993); Z. Okbani, R. Ouasti, and N. Zekri, Physica A (Amsterdam, Neth.) **234**, 38 (1996); Y. M. Liu, R. W. Peng, X. Q. Huang, Mu Wang, A. Hu, and S. S. Jiang, Phys. Rev. B **67**, 205209 (2003); L. S. Cao, R. W. Peng, R. L. Zhang, X. F. Zhang, Mu Wang, X. Q. Huang, A. Hu, and S. S. Jiang, *ibid.* **72**, 214301 (2005); Z. Zhao, F. Gao, R. W. Peng, L. S. Cao, D. Li, Z. Wang, X. P. Hao, Mu Wang, and C. Ferrari, *ibid.* **75**, 165117 (2007).

[12] X. Q. Huang, R. W. Peng, F. Qiu, S. S. Jiang, and A. Hu, Eur. Phys. J. B **23**, 275 (2001).

[13] Peter Markoš and Costas M. Soukoulis, *Wave Propagation* (Princeton University Press, Princeton, NJ, 2008).

[14] R. J. Bell and P. Dea, Discuss. Faraday Soc. **50**, 55 (1970); G. Mato and A. Caro, J. Phys.: Condens. Matter **1**, 901 (1989).

[15] M. Y. Azbel and P. Soven, Phys. Rev. B **27**, 831 (1983); C. Basu, A. Mookerjee, A. K. Sen, and P. K. Thakur, J. Phys: Condens. Matter **3**, 9055 (1991); J. B. Pendry, J. Phys. C: Solid State Phys. **20**, 733 (1987).

[16] F. Delyon, Y.-E. Lévy, and B. Souillard, Phys. Rev. Lett. **57**, 2010 (1986).
[17] Y. Wan and C. M. Soukoulis, Phys. Rev. A **41**, 800 (1990).
[18] M. I. Molina, Phys. Rev. B **58**, 12547 (1998).
[19] A. Colin Cameron and Fran A. G. Windmeijer, J. Econometrics **77**, 329 (1997); N. J. D. Nagelkerke, Biometrika **78**, 691 (1991). The determination coefficient is defined by $\rho^2 = 1 - \sigma_r^2/\sigma^2$, where σ^2 is the variance of the dependent variable and σ_r^2 is the residual variance (quadratic mean of the residues, each one being the difference between the observed and the predicted value for the variable).
[20] M. I. Molina and G. P. Tsironis, Phys. Rev. Lett. **73**, 464 (1994).